Article

Effects of Turn Stability on the Kinetics of Refolding of a Hairpin in a β-sheet

Nicole N.-W. Kuo, Joseph J.-T. Huang, Jaroslava Miksovska,
Rita P.-Y. Chen, Randy W. Larsen, and Sunney I. Chan

J. Am. Chem. Soc., **2005**, 127 (48), 16945-16954• DOI: 10.1021/ja0543191 • Publication Date (Web): 11 November 2005

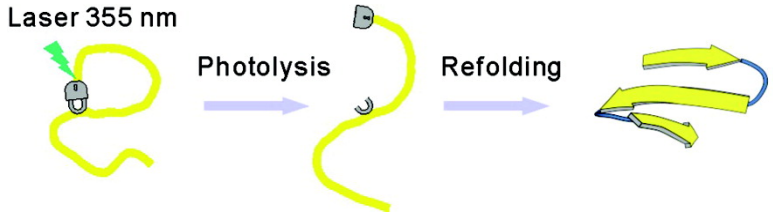

More About This Article

Additional resources and features associated with this article are available within the HTML version:

- Supporting Information
- Links to the 1 articles that cite this article, as of the time of this article download
- Access to high resolution figures
- Links to articles and content related to this article
- Copyright permission to reproduce figures and/or text from this article

View the Full Text HTML

J|A|C|S
ARTICLES
Published on Web 11/11/2005

Effects of Turn Stability on the Kinetics of Refolding of a Hairpin in a β-sheet

Nicole N.-W. Kuo,[†] Joseph J.-T. Huang,[†] Jaroslava Miksovska,[§] Rita P.-Y. Chen,[‡] Randy W. Larsen,[§] and Sunney I. Chan*,[†]

Contribution from the Institute of Chemistry, Institute of Biological Chemistry, Academia Sinica, Taipei 115, Taiwan, R.O.C., and Department of Chemistry, University of South Florida, Tampa, Florida 33620-5250

Received June 30, 2005; E-mail: chans@chem.sinica.edu.tw

Abstract: As part of our continuing study of the effects of the turn sequence on the conformational stability as well as the mechanism of folding of a β-sheet structure, we have undertaken a parallel investigation of the solution structure, conformational stability, and kinetics of refolding of the β-sheet VFIVDGOTYTEV^{D}-PGOKILQ. The latter peptide is an analogue of the original Gellman β-sheet VFITS^{D}PGKTYTEV^{D}PGOKILQ, wherein the TS^{D}PGK turn sequence in the first hairpin has been replaced by VDGO. Thermodynamics studies revealed comparable conformational stability of the two peptides. However, unlike the Gellman peptide, which showed extremely rapid refolding of the first hairpin, early kinetic events associated with the refolding of the corresponding hairpin in the VDGO mutant were found to be significantly slower. A detailed study of the conformation of the modified peptide suggested that hydrophobic interactions might be contributing to its stability. Accordingly, we surmise that the early kinetic events are sensitive to whether the formation of the hairpin is nucleated at the turn or by sequestering of the hydrophobic residues across the strand, before structural rearrangements to produce the nativelike topology. Nucleation of the hairpin at the turn is expected to be intrinsically rapid for a strong turn. However, if the process must involve collapse of hydrophobic side chains, the nucleation should be slower as solvent molecules must be displaced to sequester the hydrophobic residues. These findings reflect the contribution of different forces toward nucleation of hairpins in the mechanism of folding of β-sheets.

Introduction

Understanding the forces dominating the formation and stability of secondary structures is essential for de novo protein design and structural prediction from primary sequences. Structural analyses of protein fragments and designed peptides have contributed much to our knowledge on how α-helices are formed and stabilized.[1−5] The factors involved in the formation and stability of β-structures are more complex. Unlike α-helices, β-structures are prone to self-aggregation and, hence, not as amenable to structural studies in solution. Nevertheless, good progress has been made in recent years. Inasmuch as the propensity toward β-structure formation might be related to medical disorders such as Alzheimer's and prion diseases, there has been impetus to improve our understanding of the structural and solution properties of proteins and peptides that favor the β-structure.[6,7]

It is now widely recognized that certain specific turn sequences influence the stability of β-structures, the turn type, and even the detailed fold of the whole β-structure.[8−10] As an example, we have recently compared the stability of the β-sheet with different types of turn. As a point of departure, we have chosen the peptide designed by Gellman and co-workers (VFITS^{D}PGKTYTEV^{D}PGOKILQ, denoted as the 20mer), which has been shown to adopt an antiparallel β-sheet in aqueous solution.[11] This β-sheet is quite stable in solution and, apparently, does not undergo self-association to any appreciable extent. To examine the stability of the structure on the turn type, we have undertaken a series of mutations in the turn region and have examined the structures of these β-sheet mutants in some detail. The 20mer peptide of Gellman et al. has two ^{D}PG 2:2 type II′ turns. We have found that mutating ^{D}P-6 to D in the turn of the first hairpin (this mutant hereafter referred as the 20mer^{D}P6D peptide) did not create a peptide with the type I′ turn in the first hairpin as we had envisaged.[12] Instead, this mutation led to a structural change consisting of a one amino

[†] Institute of Chemistry, Academia Sinica.
[‡] Institute of Biological Chemistry, Academia Sinica.
[§] University of South Florida.

(1) Scholtz, J. M.; Baldwin, R. L. *Biochemistry* **1993**, *32*, 4604−4608.
(2) Lyu, P. C.; Wemmer, D. E.; Zhou, H. X.; Pinker, R. J.; Kallenbach, N. R. *Biochemistry* **1993**, *32*, 421−425.
(3) Chakrabartty, A.; Baldwin, R. L. *Adv. Protein Chem.* **1995**, *46*, 141−176.
(4) Munoz, V.; Serrano, L. *Biopolymers* **1997**, *41*, 495−509.
(5) Aurora, R.; Rose, G. D. *Protein Sci.* **1998**, *7*, 21−38.
(6) Kelly, J. W. *Nat. Struct. Biol.* **2000**, *7*, 824−826.
(7) Gorman, P. M.; Chakrabartty, A. *Biopolymers* **2001**, *60*, 381−394.
(8) Santiveri, C. M.; Santoro, J.; Rico, M.; Jimenez, M. A. *Protein Sci.* **2004**, *13*, 1134−1147.
(9) Blanco, F. J.; Jimenez, M. A.; Herranz, J.; Rico, M.; Santoro, J.; Nieto, J. L. *J. Am. Chem. Soc.* **1993**, *115*, 5887−5888.
(10) de Alba, E.; Jimenez, M. A.; Rico, M. *J. Am. Chem. Soc.* **1997**, *119*, 175−183.
(11) Schenck, H. L.; Gellman, S. H. *J. Am. Chem. Soc.* **1998**, *120*, 4869−4870.
(12) Chen, P. Y.; Lin, C. K.; Lee, C. T.; Jan, H.; Chan, S. I. *Protein Sci.* **2000**, *10*, 1794−1800.

10.1021/ja0543191 CCC: $30.25

acid frame shift in the hydrogen-bonding network and side-chain inversion on the first β-strand to yield a five-residue TSDGK turn. However, when the same substitution was made at position 14, no frame shift was noted in the resultant VDGO sequence.

As a continuation of this work, we have now introduced the VDGO turn sequence into the first hairpin for comparison with the five-residue TSDGK turn as well as the original TS^{D}PGK sequence (mutant peptide VFIVDGOTYTEV^{D}PGOKILQ, hereafter referred to as the 19mer). Aside from comparing the stability of the hairpin on the turn sequence, we have also applied the peptide "caging" strategy that we have recently developed in our laboratory to compare the fast refolding kinetics of the peptide structural elements. As shown in our recent study, this combined structural and kinetic approach affords the unique opportunity to study not only the effects of the turn sequence on the structure and conformational stability of the β-sheet but also the effects of the turn stability on the folding mechanism.

In recent years, a number of methods have been developed to observe the early stages of protein folding near the top of the "celebrated" protein-folding funnel.[13−15] Among these methods, the most popular has been the perturbed equilibrium approach evoked by the IR laser-induced T-jump method, especially when used in connection with fluorescence, IR spectroscopy and CD spectroscopy to unravel the thermal stability and folding/unfolding kinetics.[13−18] These techniques extend the time window of observation of the protein refolding process from the microsecond to the nanosecond regime. Not only the early stages, but also the formation of the molten globule could be detected. However, as a perturbed equilibrium experiment, the initial state of the protein folding process is not well-defined, and might not correspond to the randomized ensemble of unfolded states. In contrast, in the "caging" peptide strategy, a photolabile linker is used to constrain the structure of the "caged" peptide in a well-defined conformational state, and the peptide refolding starts from this initial state once the photolinker is cleaved by an ultrashort laser pulse.[19] In these experiments, we have combined the photolabile "caging" strategy with laser flash photolysis and photoacoustic calorimetry to study protein folding on the nanosecond time scale.[19−21]

Materials and Methods

Peptide Synthesis. The peptides, 20mer (sequence VFITS^{D}PGKTYTEV^{D}PGOKILQ), 20merE12C (sequence VFITS^{D}PGKTYTCV^{D}PGOKILQ), 20mer^{D}P6D (sequence VFITSDGKTYTEV^{D}PGOKILQ), 20mer^{D}P6DE12C (sequence VFITSDGKTYT CV^{D}PGOKILQ), 19mer (sequence VFIVDGOTYTEV^{D}PGOKILQ), and 19merE11C (sequence VFIVDGOTYTCV^{D}PGOKILQ) were synthesized by the batch fluorenylmethoxycarbonyl(fmoc)-polyamide method on a PS3 peptide synthesizer (Rainin). Rink amide AM resin from Novabiochem was used as the solid support. Fmoc-Cys(mmt)-OH was used because the mmt (methoxytrityl) protecting group could be cleaved under mildly acidic conditions.

To synthesize the cyclized peptide, BrAcCMB was coupled to the N-terminal end of the polypeptide chain. After the coupling was completed, the resin was treated in 1% trifluoroacetic acid/5% triisopropylsilane in dichloromethane to remove the mmt group. The cyclization was performed on the resin under basic conditions. The cyclized peptides, denoted c-20merE12C and c-19merE11C, were cleaved from the resin, purified, and identified as described in earlier publications.[21]

Aggregation Studies. The NMR spectrum of the 19mer revealed no significant changes in chemical shifts and line widths for the peptide concentration between 190 μM and 2.18 mM. This result strongly suggests that the 19mer existed as the monomer in solution under the conditions used in our 2D NMR structural analysis.

Circular Dichroism Spectroscopy. The CD spectra were recorded on a π^{*}-180 CD spectrometer (Applied Photophysics, Surrey, U.K.). Peptides were dissolved in appropriate amounts of D.I. water. CD calibration was done by using 1.5 mg/mL D-(−)-pantoyllactone at 219 nm. The data were recorded in a 1-mm cell, between 190 and 240 nm, and at room temperature. Nitrogen purge was introduced during the collection of CD data below 200 nm. A scan interval of 1 nm with an integration of 200 000 points was employed. The spectrum of D.I. water was collected as a baseline and subtracted automatically.

Nuclear Magnetic Resonance Spectroscopy. The 19mer was dissolved in 0.5 mL of H_2O/D_2O (9/1 by the volume) or D_2O at a concentration in the range of 1.4−3.4 mM. The pH of the solution was adjusted to 3.6 ± 0.1 by addition of appropriate amounts of either DCl or NaOD. The pH values were pH-meter readings and not corrected for the isotope effect. A 1/100 volume of sodium 3-(trimethylsilyl)-propionic-2,2,3,3-d_4 acid (TSP) solution (0.75% in D_2O) was added as an internal reference.

One- and two-dimensional ^{1}H NMR spectra were obtained on a Bruker AM 500 NMR spectrometer. 2D-TOCSY, NOESY, and DQF-COSY spectra were recorded by using a standard phase-cycling sequence at 280 K. The spectra were acquired with 2K data points in the direct dimension and 512 increments in the indirect dimension. A mixing time of 300 ms was used for NOESY, and a time of 80 ms was used for TOCSY. The shifted square sine-bell window function was applied in both dimensions for all spectra. Data were processed by using XWINNMR software on a Silicon Graphics workstation.

Structural Analysis. The Ansig program (version 3.3) was used to assign the NMR spectra recorded on the Bruker AM 500. To verify the formation of hydrogen bonds, the 19mer was prepared as a lyophilized powder in an NMR tube at pH 3.6. D_2O buffer was then added to the sample just prior to insertion of the NMR tube into the NMR probe for immediate data collection. 1D-spectra were collected at 5−7 min intervals for the first hour and then at 30−35 min intervals until no further changes were noted. Assignments were made for the amide protons that still persisted in the presence of the D_2O buffer after 1 h. The intensities of the intrastrand, sequential, and medium- and long-range NOEs are defined as strong (3.0 Å), medium (4.0 Å), and weak (7.0 Å) to provide the upper bound interproton distance constraints. Phi angles were restricted to $-120 \pm 30°$ for the residues with $^{3}J_{HN\alpha} > 9.5$ Hz. Structures were generated by using the program X-PLOR 98. The program INSIGHT II was used to visualize the structures. The convergence of the calculated structures was examined by the structural parameters (Table 1). The quality of the final 14 energy-minimized structures was checked with the program PROCHECK_NMR.

Method of Peptide "Caging". The peptide "caging" strategy used in the study of the refolding kinetics was based on the deployment of

(13) Munoz, V.; Thompson, P. A.; Hofrichter, J.; Eaton, W. A. *Nature* **1997**, *390*, 196−199.
(14) Thompson, P. A.; Eaton, W. A.; Hofrichter, J. *Biochemistry* **1997**, *36*, 9200−9210.
(15) Ballew, R. M.; Sabelko, J.; Gruebele, M. *Proc. Natl. Acad. Sci. U.S.A.* **1996**, *93*, 5759−5764.
(16) Maness, S. J.; Franzen, S.; Gibbs, A. C.; Causgrove, T. P.; Dyer, R. B. *Biophys. J.* **2003**, *84*, 3874−3882.
(17) Cochran, A. G.; Skelton, N. J.; Starovasnik, M. A. *Proc. Natl. Acad. Sci. U.S.A.* **2001**, *98*, 5578−5583.
(18) Dyer, R. B.; Maness, S. J.; Franzen, S.; Fesinmeyer, R. M.; Olsen, K. A.; Andersen, N. H. *Biochemistry* **2005**, *44*, 10406−10415.
(19) Hansen, K. C.; Rock, R. S.; Larsen, R. W.; Chan, S. I. *J. Am. Chem. Soc.* **2000**, *122*, 11567−11568.
(20) Rock, R. S.; Chan, S. I. *J. Org. Chem.* **1996**, *61*, 1526−1529.
(21) Chen, P.-Y.; Huang, J.-T.; Chen, H.-L.; Jan, H.; Velusamy, M.; Lee, C.-T.; Fann, W.; Larsen, R. W.; Chan, S. I. *Proc. Natl. Acad. Sci. U.S.A.* **2004**, *101*, 7305−7310.

Table 1. Structural Statistics on the Final Set of Simulated Annealed Structures of the 19mer

restraints used	
distance restraints	
intraresidue	167
sequential	44
medium and long range	36
total distance restraints	254
hydrogen bonds	5
dihedral angles	9
statistics for the final X-PLOR structures	
number of structures in the final set	14
X-PLOR energy (kcal mol^{-1})	
E_{noe}	2.85 ± 0.12
E_{cdih}	0.16 ± 0.02
$E_{bond} + E_{angle} + E_{improper}$	33.81 ± 0.24
E_{elec}	1.79 ± 0.03
E_{vdw}	9.04 ± 0.09
NOE violations	
number > 0.5 Å	none
root-mean-square deviation (Å)	0.02
deviation from idealized covalent geometry	
angle (deg)	0.55
improper (deg)	0.36
bonds (deg)	0.003
root-mean-square deviation (Å)	
backbone	
residues (all)	0.34
residues (2−18)	0.33
heavy atom(all)	0.89
Ramachandran data	
residues in most favored regions (%)	86.5
residues in allowed regions (%)	43.5
residues in generously allowed regions (%)	0
residues in disallowed regions (%)	0

3′,5′-dimethoxybenzoin as a photolabile linker to cyclize the N-terminal peptide with a cysteine introduced in the middle part of the peptide to destroy the secondary structure.[22] The 19mer containing the VDGO sequence in the first hairpin was first prepared by solid-phase peptide synthesis. In addition to introducing the new turn sequence into the first hairpin, Glu 11 was also mutated to Cys (19merE11C), and the photolabile linker bromoacetyl-carboxymethoxybenzoin (BrAcCMB) was coupled to the N-terminal of the 19merE11C by standard condensation coupling. The protecting group of Cys was then selectively removed, and the cyclization was achieved by thioester formation between the bromo group of BrAcCMB and the thio group of the Cys under mild basic condition. The cyclized peptide was finally cleaved from the resin and purified by HPLC.

To initiate the peptide refolding, the photolabile linker was cleaved by irradiation with shots of UV light from a Nd:YAG laser. The photolabile linker was cleaved within 10^{-10} s with a high quantum yield (0.72), so that the experiment had the time resolution to observe the rapid refolding of the photocleaved, linearized 19merE11C back toward its native structure. Another advantage of the benzoin photolabile linker was that the photoproduct was inert and did not interfere with or influence the collection of the kinetic data on the peptide.

Photoacoustic Calorimetry. The refolding events were detected by photoacoustic calorimetry (PAC) and photothermal beam deflection (PBD).[23] Time-resolved photothermal techniques have been wildly used in photochemistry and photobiology.[24] In PAC, one monitors the pressure wave caused by the volume expansion generated in the system on a time scale of tens of nanoseconds to several microseconds. The pressure wave arises from the volume changes that are produced by radiationless relaxation (ΔV_{th}) and structural rearrangements at the molecular level (ΔV_{con}), initiated by the pulsed laser.[23] It can be detected by fast piezoelectric transducers located in the cell plane parallel to the laser beam direction and recorded by a digital oscilloscope.

During photocleavage of the "caged" peptide and of the subsequent refolding events, heat was released (or absorbed) and the volume of the peptide and the solvent-structure changed during the structural collapse. The rate constant (k), reaction enthalpy (ΔH), volume change (ΔV_{con}), and activation energy (E_a) were derived by analyzing the time profile of the acoustic wave generated by the heat and volume changes associated with the refolding events. The high water solubility of our "caged" peptide assured that the experiment could be carried out with good sensitivity.

Peptides were dissolved in distilled water with the OD_{355} equal to 0.19. The OD_{355} of the reference potassium ferricyanide ($K_3Fe(CN)_6$) was 0.18. The sample in a 1-cm path quartz cuvette was placed in the temperature controlled cuvette holder (Flash 200, Quantum Northwest, Spokane, WA, ±0.02 °C). The excitation beam was a 355-nm output of a frequency triple Nd:YAG laser (7 ns pulse, <1500 μJ, Minilite I, Continuum, and the photoacoustic pressure wave following the laser irradiation was detected by using a piezoelectric detector with a 1-MHz bandwidth. The microphone was attached to the side wall of the cuvette parallel to the laser beam direction. The signals from the microphone were amplified by a preamplifier (Panametric 5678 preamp) and recorded by a digital oscilloscope controlled by VirtualBench-Scope software (NI5102, National Instruments). Signals from 20 laser shots were averaged.

Analysis of Photoacoustic Signals. The photoacoustic signal detected at the microphone can be described by

$$S = KE_A\Phi(\Delta V_{th} + \Delta V_{con}) \tag{1}$$

where K is instrumental response parameter, E_A is the number of Einsteins absorbed, and Φ is the quantum yield. ΔV_{th} and ΔV_{con} represent the volume change generated by thermal and conformational contribution, respectively. Because of ΔV_{th} is equal to $Q^*(\beta/C_p\rho)$, the equation could be rewritten to

$$S_{sam} = KE_A\Phi\left(Q^* \frac{\beta}{C_p\rho} + \Delta V_{con}\right) \tag{2}$$

where Q is the heat released, β is the coefficient of thermal expansion of the solution (K^{-1}), C_p is the specific heat capacity (cal g^{-1} K^{-1}), and ρ is the density (g mL^{-1}). Photocalorimetric reference compounds are usually substances that are nonfluorescent, photochemically stable, and 100% efficient in delivering the absorbed energy to the medium as heat ($\Phi_{ref} = 1$) when the excited molecules return to their ground state. Therefore, the signal for the reference can be described as

$$S_{ref} = KE_AE_{h\nu}\left(\frac{\beta}{C_p\rho}\right) \tag{3}$$

where $E_{h\nu}$ is the energy of the absorbed light. The ratio of the signal amplitude of the sample to that of the reference reflects the exact properties of the sample:

$$\frac{S_{sam}}{S_{ref}} = \frac{\Phi}{E_{h\nu}}\left[Q + \frac{\Delta V_{con}}{F(t)}\right] \tag{4}$$

where $F(t) = (\beta/C_p\rho)$. This equation could be rearranged to

$$\frac{S_{sam}}{S_{ref}}E_{h\nu} = \Phi\left[Q + \frac{\Delta V_{con}}{F(t)}\right] \tag{5}$$

A plot of (S_{sam}/S_{ref}) versus ($C_p\rho/\beta$) should give a straight line with a slope equal to ΦV_{con} and an intercept equal to the heat released (ΦQ). From $E_{h\nu}$ and the intercept, we can derive the ΔH for the reaction.

(22) Chan, S. I.; Huang, J. J.-T.; Larsen, R. W.; Rock, R. S.; Hansen, K. C. In *Dynamic Studies in Biology*; Goeldner, M., Givens, R., Eds.; Wiley-VCH Verlag GmbH & Co. KGaA: Weinheim, 2005; pp 479−494.
(23) Miksovska, J.; Larsen, R. W. *J. Protein Chem.* **2003**, *22*, 387−394.
(24) Gensch, T.; Viappiani, C. *Photochem. Photobiol. Sci.* **2003**, *2*, 699−721.

The observed time-dependent acoustic signal $S(t)$ is produced by the convolution of a time-dependent function of the decay process $H(t)$ with an instrument response function $R(t)$, which reflects the response of the transducer to a pressure wave whose duration is shorter than 30 ns and can be independently determined from the reference compound:

$$S(t) = \int R(t - t')\, H(t')\, dt' \tag{6}$$

where

$$H(t) = \phi_1 e^{-t/\tau_1} + \phi_2 e^{-t/\tau_2} + \cdots \tag{7}$$

The PACW98V1 software developed in Dr. Larsen's laboratory was used to obtain parameters ϕ_i and k_i ($k_i = 1/\tau_i$; $\phi_i = S_{sam}/S_{ref}$). Deconvolution of the signal involves estimation of the parameters ϕ_i and τ_i for $H(t)$ function with the $R(t)$ function to produce an estimated $S(t)$. The parameters ϕ_i and τ_i are varied until the estimated $S(t)$ fits the $S(t)_{obs}$. Processes occurring faster than roughly 30 ns cannot be resolved, but the integrated enthalpy and volume changes can be quantified from the amplitude of the acoustic wave. The temperature dependence of the rate constants could be analyzed by the following relationships:

$$k = k_0 e^{-E_a/RT} \tag{8}$$

$$\ln k = \ln k_0 - E_a/RT \tag{9}$$

where $k = 1/\tau$. The activation energy (E_a) and the pre-exponential factor k_o could then be derived from a linear plot of ln k vs $1/T$ (Arrhenius plot).

Results

In our earlier work,[12] we have shown that the 20mer^{D}P6D peptide differs from the original Gellman peptide by having a new five-residue turn in the N-terminal hairpin with new hydrogen-bond pairing (Figure 1). In contrast, the similar mutation at the other hairpin (^{D}P-14 to D) led to a type I′ turn for the VDGO sequence in the peptide with the double mutation (20mer^{D}P6D/^{D}P14D peptide). NMR data suggested that the side-chain pairings were not altered between the second and third strands, although it was evident from the observed interstrand NOEs that the new turn was not as tight as the original one. The peptide with the ^{D}P−G turn possessed the side-chain pairings V-to-E, F-to-T, I-to-Y, T-to-T, and S-to-K. Upon substituting Asp for ^{D}Pro at the N-terminal hairpin, the first strand of the β-sheet shifted one residue toward the turn and formed a five-residue TSDGK turn stabilized by the side-chain pairings V-to-T, F-to-Y, I-to-T, and T-to-K. Evidently, the SDGK sequence cannot form a turn as strong as the ^{D}P−G turn, and it is necessary to give up one residue in order to stabilize the turn.

Based on the previous observation that the VDGO sequence forms a type I′ turn in the second hairpin of the 20mer^{D}P6D/^{D}P14D peptide, we have prepared in the present study the corresponding peptide with the VDGO sequence introduced into the turn of the first hairpin, in place of the original TS^{D}PGK sequence of the 20mer. Since the 19mer peptide is one amino acid shorter than the original Gellman peptide or the 20mer^{D}P6D peptide, it is possible for the side-chain pairings to change in the first hairpin. If the side-chain pairings are similar to those in the first hairpin of the 20mer^{D}P6D, it might indicate that these side-chain pairings are the stable ones, and the side-chain pairings in the 20mer are due to the ^{D}PG turn (Figure 1). If the first hairpin becomes unfolded, it would suggest that the TSDGK turn is the origin of the strand flip.

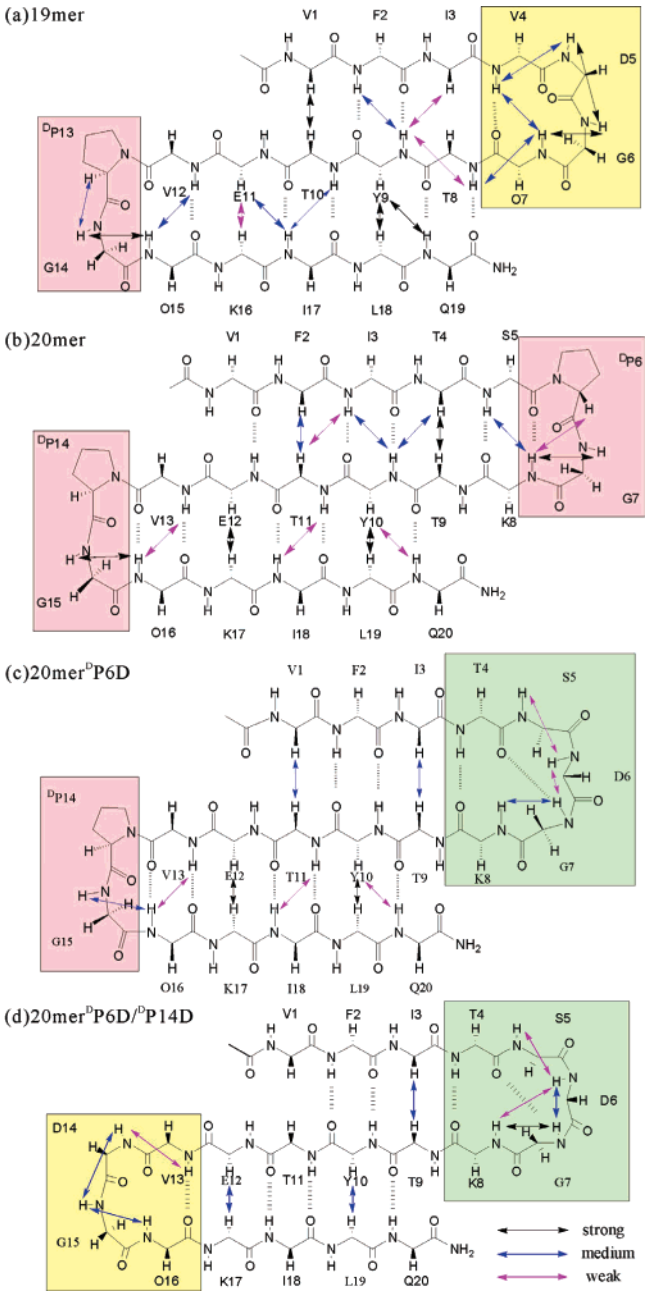

Figure 1. Backbone NOEs observed in the NOESY spectrum of (a) 19mer, (b) 20mer, (c) 20mer^{D}P6D, and (d) 20mer^{D}P6D/^{D}P14D at pH = 3.6 and 280 K. $H^{\alpha}-H^{\alpha}$ NOEs were measured in D_2O, while the remaining NOEs were measured in 9:1 H_2O/D_2O. O = ornithine.

Evidence that Peptide 19mer Adopted a Three-Stranded Antiparallel β-Sheet Structure. ^{1}H NMR data acquired at 500 MHz revealed an abundance of backbone−backbone NOEs at 280 K. Part of the NOESY spectra of the 19mer is shown in Figure 2. The spectra were fully assigned using NOESY and TOCSY. Based on the long-range NOEs, including $d_{\alpha\alpha}$ cross-peaks between 1V−10T, 11E−16K, and 9Y−18L; $d_{\alpha N}$ cross-peaks between 3I−9Y, 9Y−19Q, and 11E−17I; d_{NN} cross-peaks between 2F−9Y, 4V−7O, 10T−17I, and 12V−15O; and a multitude of d_{sc-sc} cross-peaks, it is evident that the 19mer has adopted a three-stranded β-sheet. From the NOEs observed for

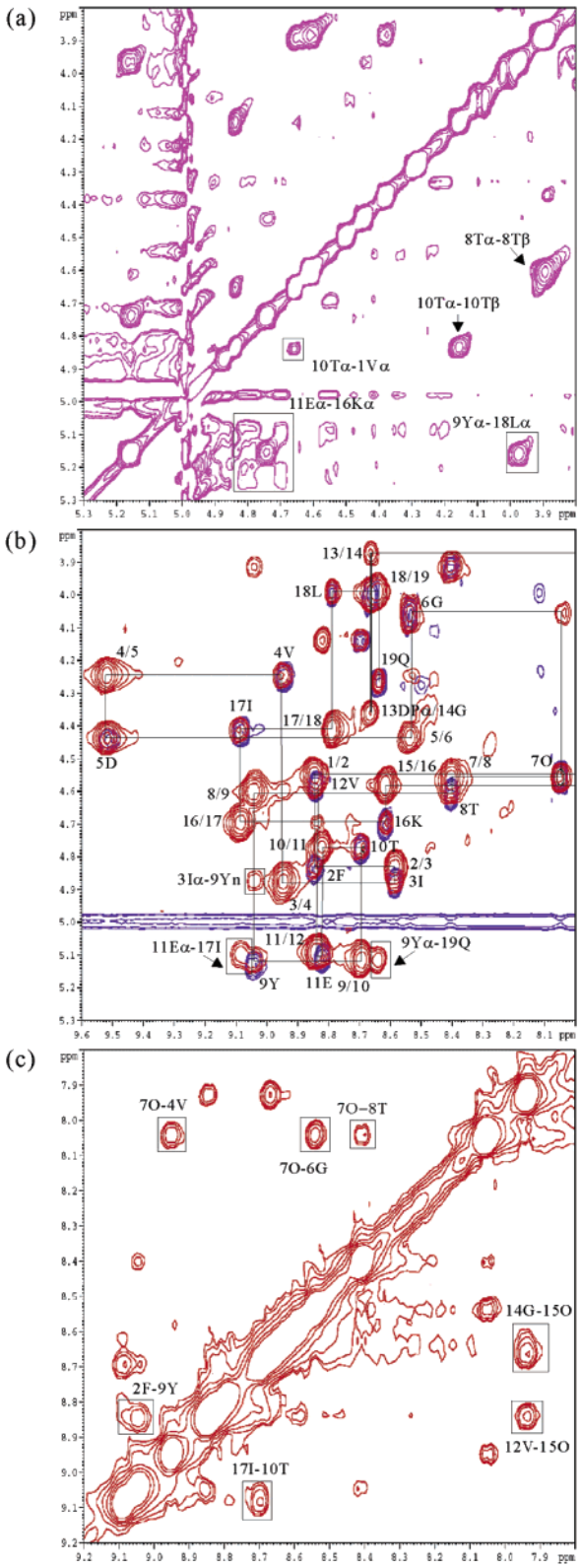

Figure 2. Selected regions of the NOESY spectra of the 19mer at 280 K. (a) $H^{\alpha}-H^{\alpha}$ region in D_2O at pH = 3.7 (1.44 mM); (b) $H^{\alpha}-NH$ region and; (c) NH−NH region in 1:9 D_2O/H_2O at pH = 3.6 (3.3 mM). The sequential connectivities are annotated.

the first turn region (d_{NN} cross-peaks between 4V−5D, 5D−6G, 6G−7O), we have concluded that the first turn has adopted a type I′ turn (Figure 1), just as the corresponding turn in the second hairpin of the 20mer^{D}P6D/^{D}P14D.

Additional evidence for β-sheet formation was obtained from the chemical shifts of α-protons, which are sensitive to secondary structure. Structural information was provided by the α-proton chemical shift index defined by $\Delta\delta_{\alpha H} = \delta_{\alpha H(\text{observed})} - \delta_{\alpha H(\text{random coil})}$.[25] A positive $\Delta\delta_{\alpha H}$ suggested a higher proportion of β-sheet, and a negative $\Delta\delta_{\alpha H}$ was consistent with a higher proportion of α-helix. The comparison of the $\Delta\delta_{\alpha H}$ values of the 19mer with those of other peptides is shown in Figure 3. When there were three or more consecutive residues with $\Delta\delta_{\alpha H}$ values bigger than 0.1 ppm, the peptide segment could be assigned to the β-sheet conformation. The negative $\Delta\delta_{\alpha H}$ value observed for L18 most likely arose from the ring current effect from the nearby aromatic side chain of Y9 in the folded state.

To check the rigidity of the structure and identify the hydrogen bonds, we have performed measurements of the amide proton exchange rates on the 19mer using one-dimension NMR. The amide protons of 1V, 3I, 4V, 12V, and 17I were still present in the peptide after incubation in D_2O for more than 60 min, suggesting that these residues were likely involved in strong hydrogen bonds (data not shown). We have exploited this information and have invoked these hydrogen bonds as input into our structural calculations in an attempt to obtain an accurate structural geometry of the 19mer. In addition, we have made extensive use of coupling constant data in the structural calculations. The local structural parameter $^{3}J_{HN\alpha}$ was estimated from two-dimensional double quantum filtered correlated spectroscopy. These coupling constants were bigger than 9.5 Hz for residues 1V, 2F, 3I, 4V, 8T, 9Y, 10T, 12V, 14G, 15O, 17I, and 19Q. Accordingly, these residues should be in the β-conformation, and we have restricted the torsional ϕ angles in these residues to $-120 \pm 30°$ in the structural calculations.

Finally, the NMR data indicated that the three-stranded β-sheet conformation of the 19mer peptide was significantly populated in aqueous solution in our experiments. The observation of a significant number of long-range main-chain NOEs is consistent with this conclusion. These NOEs are summarized in Figure 4.

A set of 268 restraints was used for simulating and minimizing the structure using the software program X-PLOR. Among these restraints, 254 were interproton distance restraints, 5 were hydrogen bonds, and 9 were dihedral angles. The calculated structures were checked according to the root-mean-square deviations from the idealized geometry, total energy, and distance violations. Fourteen structures were chosen to present the ensemble of NMR structures on the basis of minimal distance and torsion angle restraint violations in the final stage. All of these structures were consistent with both experimental data and standard covalent geometry and displayed no distance restraint violations greater than 0.5 Å. Superposition of the backbones (N, C_{α}, and C′) for the 14 structures from residues 2−18 revealed an averaged root-mean-square deviation of only 0.33 Å. PROCHECK analysis revealed that none of the residues were in disallowed regions of the Ramachandran plot (data not shown). The structural statistics in the final set of structures are given in Table 1.

19mer Adopted a Right-Handed Twist. From the stereoscopic view of the superimposed 14 structures calculated for the β-sheet in water, the 19mer is a right-handed twisted

(25) Bundi, A.; Wuthrich, K. *Biopolymers* **1979**, *18*, 285−297.

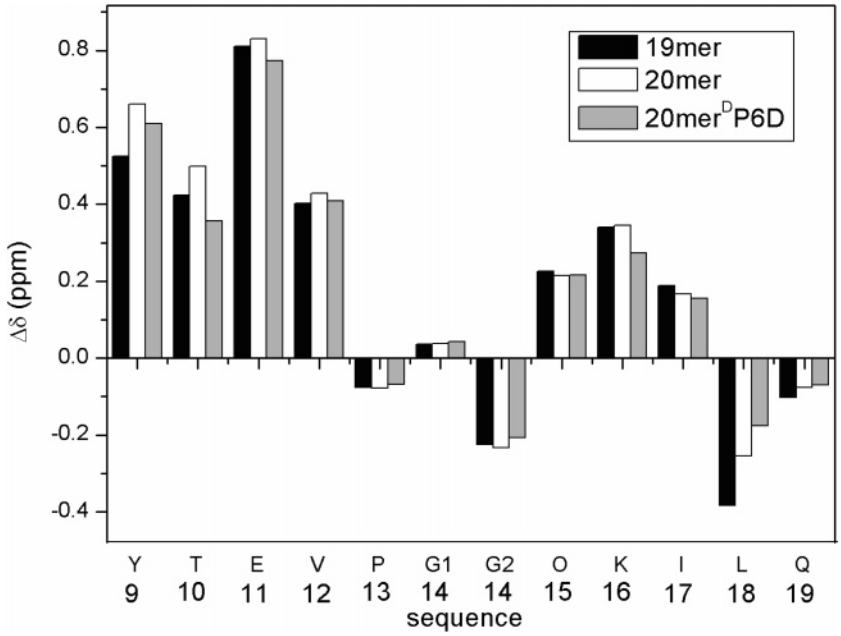

Figure 3. A plot of the deviations of the H^{α} chemical shifts of the 19mer, 20mer, and 20mer^{D}P6D from the random coil values. The NMR spectra were recorded in 9:1 H_2O/D_2O pH = 3.6 and 280 K. The amino acid sequence from 9Y to 19Q of the 19mer is shown on the *x*-axis. The two α-protons of glycine are denoted by G1 and G2. ($\Delta\delta_{\alpha H} = \delta_{\alpha H}$(observed) $- \delta_{\alpha H}$(random coil)). The reported random coil value for lysine was used for ornithine because it has been shown that the $\delta_{\alpha H}$ of ornithine is very close to that of lysine. Black bar, 19mer; white bar, 20mer; gray bar, 20mer^{D}P6D.

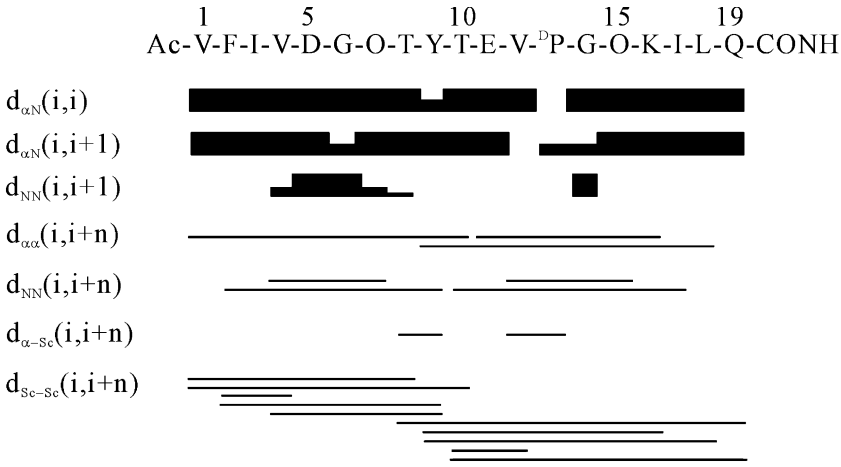

Figure 4. Summary of the NOE data for the *β*-sheet in aqueous solution at 280 K, pH = 3.6. The relative NOE intensities were estimated from the cross-peak intensities and used subsequently in the structure calculations.

structure (Figure 5). The right-handed twist is supported by the NOEs observed for the following side-chain protons: (1) the diagonal *i*, *j* ± 2 between the first to second strand and the second to third strand (*j* is the opposite residue of *i*); (2) between the *i*, *i* + 2 residues; and (3) the side-chain backbone other than *i*, *j*, or *i*, *i* + 2 residues (Figure 4).[8] There are several hydrophobic residues that might contribute to the twist, for example, the hydrophobic cluster formed among 2F, 4V, 9Y, and 16K (Figure 6).

Structural Stability of the 19mer vs the 20mer. The CD spectrum of the 19mer at ambient temperatures in aqueous solution displayed a maximum negative ellipticity at around 218 nm and a strong positive ellipticity at around 202 nm, characteristic of *β*-sheet structure. The decrease in ellipticity at 202 nm with increasing temperature suggested loss of secondary structure at higher temperatures (Figure 7).

Despite the different turn type at the first hairpin between the 19mer (a type I′ turn) and the 20mer (type II′ turn), the thermodynamic stabilities of the two peptides are similar, when their thermal denaturation curves are compared (Figure 7). This conclusion is corroborated by the chemical shift index of these two peptides. Because the ^{D}PG turn in the 20mer is a more stable turn than the VDGO turn in the 19mer, it follows that the hydrophobic interactions among the side-chain pairings must be contributing more to the stability of the 19mer than the 20mer. Accordingly, we surmise that the side-chain pairings observed for the 20mer must be imposed by the dominating ^{D}PG turn and that the frame shifts observed for the 20mer^{D}-P6D and 19mer peptides must be driven by the favorable side-chain interactions. In support of this view, visual inspection of our structures of the 19mer revealed a hydrophobic cluster: involving 2F, 4V, 9Y and 16K (Figure 6). It is likely that this hydrophobic cluster provides for the structural stability of the 19mer peptide.

Folding Kinetics of the 19mer. We have recently reported the application of the "caged" peptide strategy and PAC to the

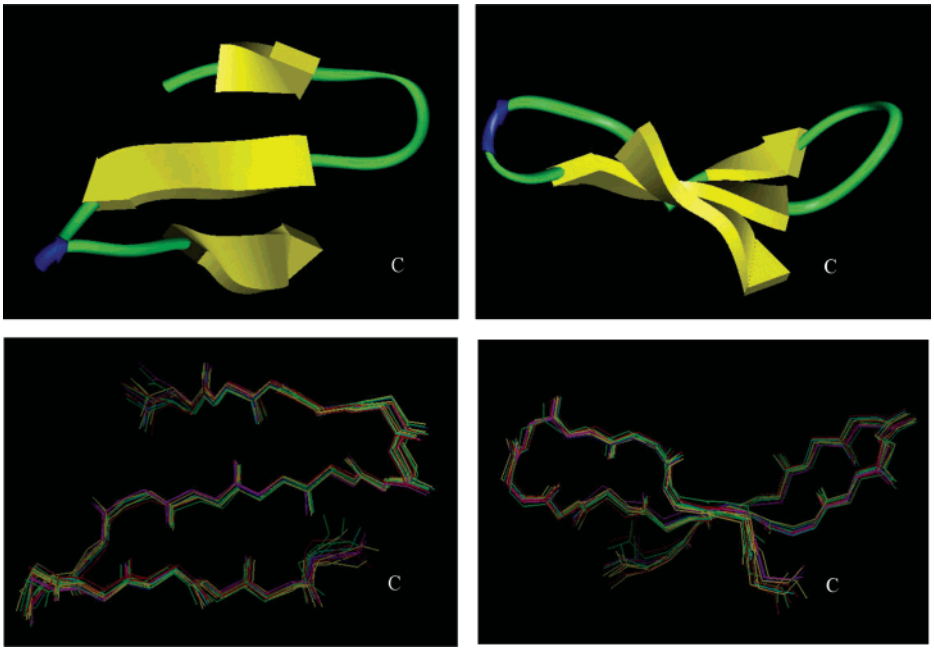

Figure 5. Stereoplots of the superimposition of the backbone of the best 14 structures calculated for the 19mer. The RMSD from the mean structure for residues 2 to 18 is 0.33 Å. The "C" label indicates the carboxy-terminus.

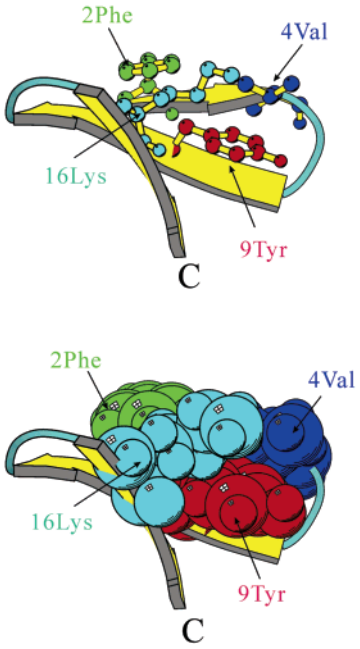

Figure 6. Visual inspection of the 19mer structure reveals a hydrophobic cluster involving 2F, 4V, 9Y, and 16K.

study of the folding kinetics of several structural motifs, including α-helices, hairpins, and β-sheets.[19−21] It has been found that the formation of secondary structures occurs on a nanosecond to microsecond time scale.[22,26] For example, α-helices refold at time scales of the order of 10 ns (dead time of the method), and β-sheets at times from 10 ns to microseconds, depending on the thermodynamic stability of the turns. When the strategy was applied to the Gellman peptide, the refolding took place with a time constant of 40 ns.[21] When it was applied to the 20mer^{D}P6D peptide, the refolding was biphasic consisting of a fast phase with a time constant of 40 ns and a slower phase with a time constant of 150 ns.[21] Advantages of the "caged" peptide strategy are that the protein folding is initiated from a well-defined initial state, and the process is irreversible once the photolabile linker is cleaved to trigger the refolding process.

Here, we have compared the refolding kinetics of the 19mer with that of the 20mer. A cyclized peptide c-19merE11C was prepared, cyclized at the exactly same position as in the case of the c-20merE12C. The refolding kinetics of the cyclized peptide was followed by photoacoustic calorimetry (PAC) as shown in Figure 8a, where we have overlaid the acoustic waves from photocleavage of the c-19merE11C and photoexcitation of the reference at 20 °C. The larger amplitude of the sample acoustic trace and its phase shift to lower frequencies relative to the reference trace indicate the presence of kinetic processes between ∼40 ns and ∼10 μs. The PACW98V1 software was used to resolve amplitudes (ϕ_i) and the lifetime (τ_i) for each process. During the data fitting, the lifetime of the fast process was fixed to be 1 ns reflecting volume and enthalpy changes that occur faster than the resolution of our instrument. The amplitudes and the time constants associated with subsequent phases were obtained by deconvolution of the sample trace. Two phases were required for the fitting of the photoacoustic wave observed for the c-19merE11C. The first phase was described by a process with $\phi_1 = 0.50$ and $\tau_1 = 1$ ns. The second phase was characterized by $\phi_2 = -0.569$ and $\tau_2 \approx 600$ ns at 20 °C. The first kinetic event corresponded to the cleavage of the linker, and the second, the refolding of the c-19merE11C.

The quality of the fit by the kinetic parameters ϕ_1, τ_1, ϕ_2, and τ_2 is shown in Figure 8a. The red line shows a simulation based on the kinetic parameters derived. Deviations between the simulated wave and the experimental wave are given as residuals of the fitting, which are plotted as the dotted trace. The low residuals suggest that the fit is excellent.

The present study of the refolding kinetics indicates that the refolding of the c-19merE11C ($\tau \approx 600$ ns) is much slower

(26) Bieri, O.; Kiefhaber, T. *Biol. Chem.* **1999**, *380*, 923−929.

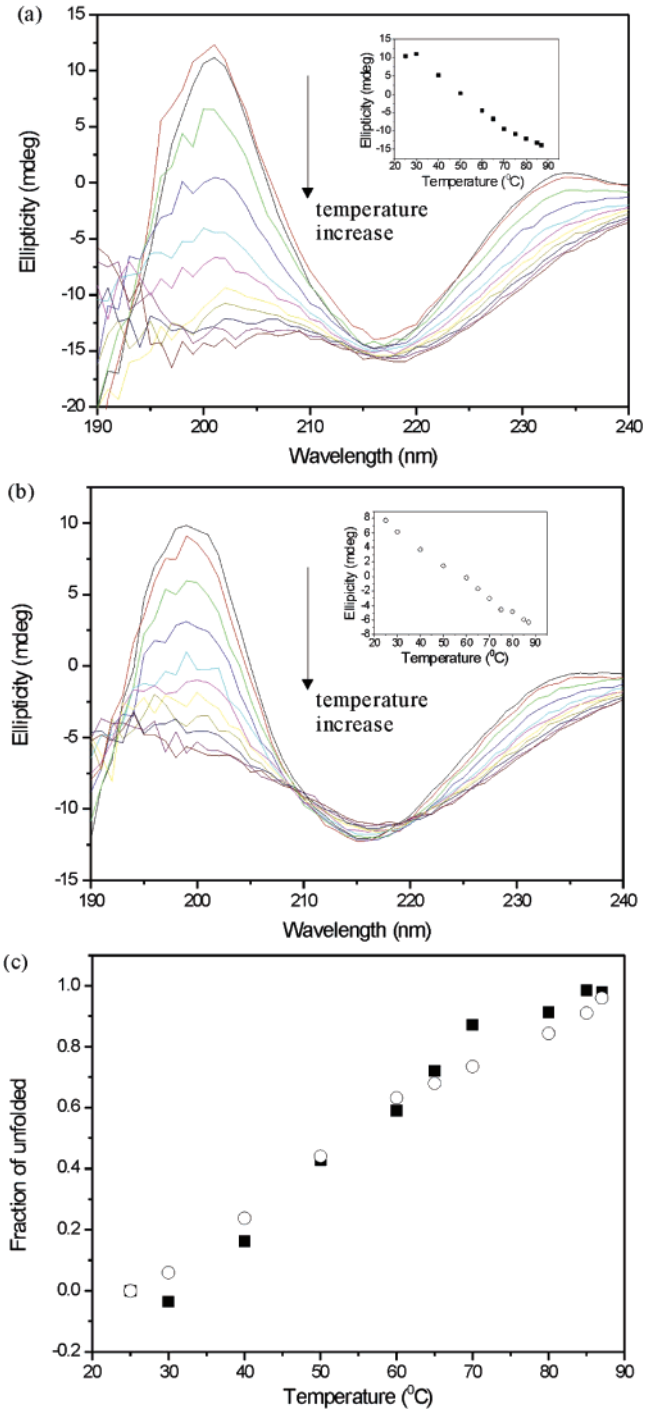

Figure 7. CD spectra of the 20mer and 19mer. Peptide concentrations were about 70 μM. Ellipticity at 202 nm of the 19mer and 20mer decreased with increasing temperature (a and b, respectively). The insets depict the ellipticity at 202 nm at different temperatures. (c) Thermal denaturation curves of the 19mer (■) and 20mer (○) in H_2O.

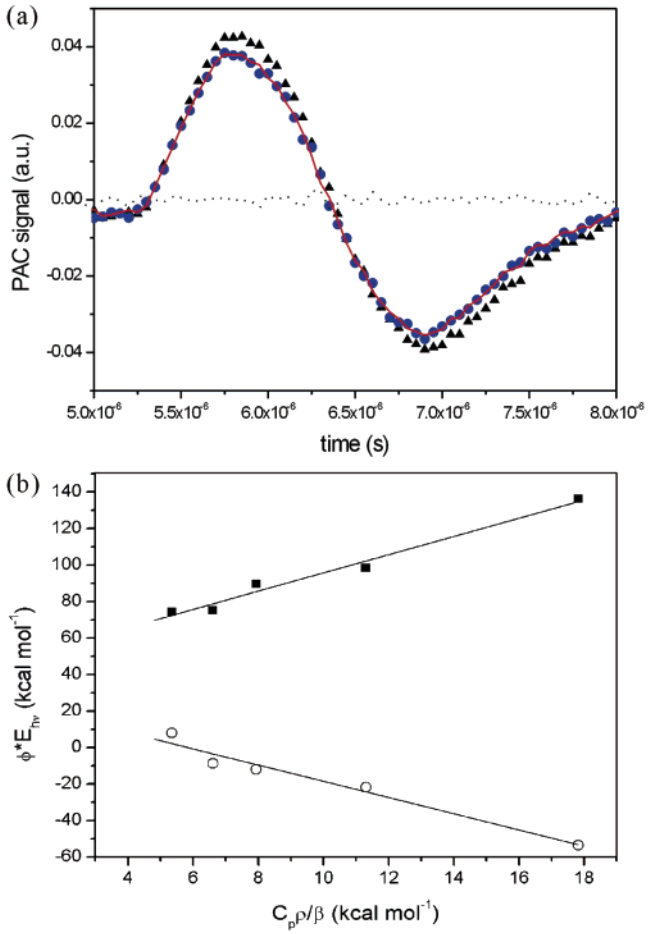

Figure 8. (a) The photoacoustic wave generated by laser irradiation of the c-19merE11C. The signals from the peptide sample and the reference compound are shown as blue circles and black triangles, respectively. The simulated result is shown by the red line. The residuals are given by the dotted trace. (b) From plots of $\phi^*E_{h\nu}$ versus $C_p\rho/\beta$ for the fast phase (■) and slow phase (○), we can obtain Q, ΔH, and ΔV from the temperature dependence of the photoacoustic signals.

than the c-20merE12C ($\tau \approx 40$ ns) and the c-20mer^{D}P6D peptide ($\tau \approx 150$ ns). In a separate study, we have also monitored the refolding kinetics using PBD. Although conformational dynamics and enthalpy changes could be studied by using both photoacoustic calorimetry and photothermal beam deflection, the two methods have different observation time domains. While the PAC could measure enthalpy/volume changes occurring from 40 ns to 10 μs, the PBD could measure volume/enthalpy changes occurring from roughly 10 μs to 5 ms. In PBD, the density change arises from the volume change brought about by the thermal heating of the solvent. The density change causes a change in the refractive index which changes the propagation direction of the probe beam. The magnitude of the change is directly proportional to the amount of sample heating and/or molar volume change. Further details of the method as well as analysis of PBD data are given in a recent paper from the Larsen group.[23] Since the PBD signal from the c-19merE11C peptide overlapped with that of the reference (Supporting Information), there is evidently no other later event in the refolding.

Temperature Dependence of the Refolding Kinetics. We have examined the refolding kinetics of the c-19merE11C peptide over a narrow temperature range. Temperature-dependent acoustic signals recorded between 7 °C and 20 °C are shown in Figure 9a. The acoustic waves of the sample were found to be shifted in phase relative to the reference acoustic waves. These data enabled a plot of $\phi_i^*E_{h\nu}$ vs $C_p\rho/\beta$, from which the volume change accompanying the events associated with each phase could be deduced from the slope and the heat released to the solution from the intercept, according to eq 5 (Figure 8b). The enthalpy (ΔH) of the reaction for the fast phase could be calculated from the heat released (Q), where $\Phi \cdot \Delta H = E_{h\nu} - Q$ and $\Phi = 0.72$ for Br-AcCMB. The enthalpy (ΔH) of the

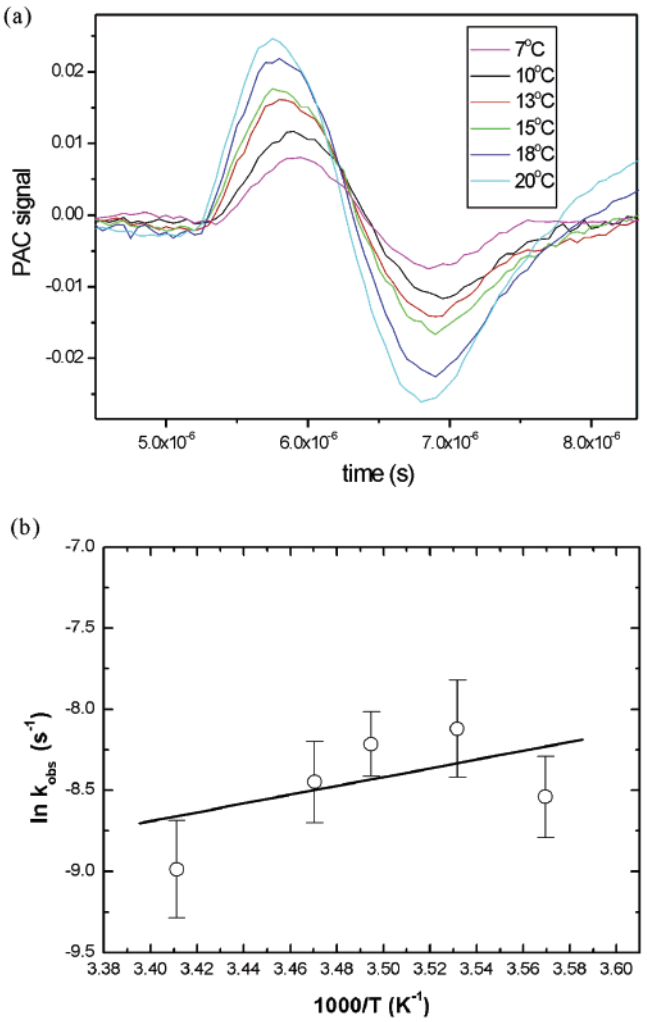

Figure 9. (a) Temperature dependence of the sample photoacoustic signal in water. Acoustic waves were obtained at 7, 10, 13, 15, 18, and 20 °C in separate experiments. (b) Arrhenius plot for the rate constants obtained for the slow phase of the c-19merE11C.

reaction for the slow phase could also be calculated from the released heat (Q) of the slow phase, where $\Phi \cdot \Delta H = -Q$. The fast process exhibited a volume expansion (ΔV) of 6.9 ± 0.5 mL mol^{-1} and the corresponding enthalpy change ($\Delta H = (E_{hv} - Q)/\Phi$) was 48 ± 6.2 kcal mol^{-1}. The fast process was followed by a slower reaction with a volume contraction of $\Delta V = -6.25 \pm 0.6$ mL mol^{-1}, and the enthalpy change ($\Delta H = -Q/\Phi$) is −36 ± 7.5 kcal mol^{-1}. Clearly, the fast phase represents essentially the breakage of the linker: the volume change for this phase is positive, and the reaction is endothermic. The observed positive enthalpy change is consistent with the breakage of the photolabile linker, and the volume change is contributed from the exposure and solvation of the hydrophobic residues after photocleavage of the linker. However, we cannot exclude that initial folding events occurring within 20 ns are also contributing to the volume and enthalpy changes for the fast phase. The slow phase corresponds to the refolding of the peptide: the volume change and the enthalpy change are both negative. The net volume decrease reflects the contraction arising from the structural collapse as well as reburial of hydrophobic residues. Evidently, the slow phase of the c-19merE11C is driven both enthalpically and entropically, with contributions from the formation of hydrogen bonds as well as the hydrophobic collapse to form the hydrophobic cluster observed in the structure.

The activation energy (E_a) of the folding process was also calculated from the temperature dependence of the rate constant associated with the slow phase ($k_{obs} = 1/\tau_2$) according to eq 8. The plot of ln k_{obs} vs $1/T$ is shown in Figure 9b and gives the activation energy $E_a = -1.8 \pm 0.4$ kcal mol^{-1}, essentially zero.

Discussion

^{D}PG adopts the 2:2 type II′ turn, TSDGK adopts the 3:5 type I plus a β-bulge, and VDGO adopts the type I′ turn (Figure 1).[12] Type I′ and II′ are the more common turn types in hairpins, though not in proteins.[27−29] Type I′ and II′ turns are generally associated with 2:2 hairpins and a geometry matching the right-handed twist. The extra bulge residue often follows a type I turn to release strain when a 3:5 turn is formed. From protein structure databases, it has been shown that Gly is the most prevalent residue at the second position, and Asn, Asp, or Gly is the most frequently encountered residue at the first position of a two-residue type I′ turn.[30−33] In a similar analysis of X-Gly type I′ turn sequences found in protein structures, Ramirez-Alvarado et al. have also concluded that there is a strong statistical preference for having Asp or Asn in the first position, followed by Gly.[34] When Gly is at the second position of the turn, it is commonly followed by a Lys. There is a propensity of having a charged residue at this position.[35] Bulky hydrophobic residues are common at the position preceding the turn, and Val is the most prevalent, although residues with polar side chains are not excluded. Thus, the turn sequence VDGO used here incorporates many of the important features identified by the statistical analysis.

In our previous paper,[12] we showed that different turn types can affect the stability of the β-sheet with the same strand sequence. Our 20mer and 20mer^{D}P6D have the same strand sequence but different turn sequence, so the stability is different. The 20mer has a strong turn, and it works like a clamp to stabilize the formation of the hairpin. In contrast, the 20mer^{D}-P6D has a weaker turn, and it is stabilized by a frame shift to form a five-residue turn structure with altered side-chain pairings between the first two strands.

Recently, we have compared the refolding kinetics between the 20mer and the 20mer^{D}P6D β-sheets using the "caged" peptide flash photolysis strategy developed in this laboratory.[21] A single process was observed in the PAC for the c-20merE12C with a time constant of 40 ns at 20 °C; two processes were observed for the c-20mer^{D}P6DE12C with time constants of 40 ns and 150 ns at 20 °C. Evidently, the refolding of the β-sheet is extremely rapid; and the stronger the turn, the faster the overall process.

(27) Chou, P. Y.; Fasman, G. D. *J. Mol. Biol.* **1977**, *115*, 135−175.
(28) Lewis, P. N.; Momany, F. A.; Scheraga, H. A. *Biochim. Biophys. Acta* **1973**, *303*, 211−229.
(29) Sibanda, B. L.; Thornton, J. M. *Nature* **1985**, *316*, 170−174.
(30) Bernstein, F. C.; Koetzle, T. F.; Williams, G. J.; Meyer, E. F., Jr.; Brice, M. D.; Rodgers, J. R.; Kennard, O.; Shimanouchi, T.; Tasumi, M. *J. Mol. Biol.* **1977**, *112*, 535−542.
(31) Sibanda, B. L.; Thornton, J. M. *Methods Enzymol.* **1991**, *202*, 59−82.
(32) Griffiths-Jones, S. R.; Sharman, G. J.; Maynard, A. J.; Searle, M. S. *J. Mol. Biol.* **1998**, *284*, 1597−1609.
(33) Griffiths-Jones, S. R.; Maynard, A. J.; Searle, M. S. *J. Mol. Biol.* **1999**, *292*, 1051−1069.
(34) Ramirez-Alvarado, M.; Blanco, F. J.; Niemann, H.; Serrano, L. *J. Mol. Biol.* **1997**, *273*, 898−912.
(35) Ramirez-Alvarado, M.; Blanco, F. J.; Serrano, L. *Nat. Struct. Biol.* **1996**, *3*, 604−612.

When the formation of a hairpin or a β-sheet is nucleated in the vicinity of the turn, the kinetics is expected to be extremely rapid as the process is driven by local forces at the turn site. For a strong turn, as in the case of the 20mer, the formation of the turn guides the subsequent assembly of the final structure.[21] For a hairpin or a β-sheet with a weaker turn, or one that is also stabilized by hydrophobic interactions across the strand, the process can be expected to be slower and more complex, as in the case of the c-20mer^{D}P6DE12C peptide. For an even weaker turn so that the turn formation must necessarily be nucleated by interactions of the hydrophobic residues across the strand, the kinetics must be even slower, as solvent molecules must be displaced to sequester the hydrophobic residues. This is apparently the case in the c-19merE11C, where the refolding of the peptide following photocleavage of the c-19merE11C occurred at the significantly slower constant of ~600 ns. Here, the 19mer formed a stable right-handed type I′ β-sheet with the same side-chain pairings as the 20mer^{D}P6D peptide. However, as highlighted by the stereoview in Figure 6, F2, V4, Y9, and K16 are docked closely in the final structure and these residues must contribute significantly to the stability of the 19mer. In other words, the first hairpin is stabilized primarily by hydrophobic interactions between F2, V4, and Y9 in the first and second strands, and the second hairpin is stabilized by the ^{D}PG turn as well as by the hydrophobic interactions between Y9 and K16 in the second and third strands, respectively. Recently, Dyer et al. have explored the folding kinetics of the peptides with the stabilizing hydrophobic cluster connected by loops of different lengths. They found that the β-hairpin formation is substantially accelerated when the connecting loop is shorter because of the entropic cost in the loop search.[36] In the case of our c-19merE11C, although its length is one residue shorter than the c-20merE12C and c-20mer^{D}P6DE12C peptides, its refolding rate is actually slower. That is because their folding pathways are actually driven by different forces. The c-20merE12C and c-20mer^{D}P6DE12C peptides have the sequence with a stronger proclivity in populating a turn sequence in the first hairpin, while the hairpin formation in the c-19merE11C peptide is assisted by the long-range hydrophobic interactions.

The time constant of the refolding observed for the 19mer peptide is of the same order as that observed for other hydrophobic hairpins with corresponding weak turn structures. So the refolding of the β-hairpin or the β-sheet must be "nucleated by hydrophobic collapse followed by rearrangements to produce a nativelike topology".[37] Muñoz et al. [13] have reported a refolding study of the β-hairpin peptide GEWTY-DDATKTFTVTE from the protein G B1 domain by a nanosecond laser temperature-jump apparatus. The folding time constant of the β-sheet was 6 μs, even slower than that observed for the 19mer in the present study. More recently, Gai et al. have extended the study to other tryptophan zippers from the protein G B1 domain[17,38] and concluded that "a stronger turn-promoting sequence increases the stability of a β-hairpin primarily by increasing its folding rate, whereas a stronger hydrophobic cluster increases the stability of a β-hairpin primarily by decreasing its unfolding rate".

The findings summarized here extend the results of our recent study on the refolding kinetics of two β-sheets with relatively strong turn structures to the refolding kinetics of a β-sheet with a significantly weaker turn. Together, the two studies illustrate the interplay between turn stability and cross-strand hydrophobic clustering in influencing the mechanism and kinetics of refolding of a β-sheet.

Conclusions

We have studied the structure, conformational stability, and refolding kinetics of the β-sheet peptide VFIVDGOTYTEV^{D}-PGOKILQ. This three-stranded β-sheet differs from the β-sheet VFITS^{D}PGKTYTEV^{D}PGOKILQ that we had previously examined[12,21] in that the TS^{D}PGK turn sequence in the first hairpin has been replaced by VDGO. The structural studies revealed that the turn in the first hairpin is considerably weaker, but the structure is otherwise stabilized by the cross-strand hydrophobic interactions. Consistent with these structural findings, the refolding kinetics is significantly slower, 600 ns for the hairpin with the weaker turn compared to 40 ns previously measured for the β-sheet with the stronger TS^{D}PGK turn sequence. These differences in the kinetics of refolding of the two β-sheets reflect the contribution of different forces toward nucleation of hairpins in the mechanism of folding of β-sheets. Nucleation of a hairpin at the turn is expected to be intrinsically rapid for a strong turn, as the process is driven by local forces at the turn site. For a hairpin with a weaker turn, the process must involve collapse of hydrophobic side chains across the strands, and the nucleation should be slower as solvent molecules must be displaced to allow sequestering of the hydrophobic residues.

Acknowledgment. We thank Dr. C.-S. Hsu for his assistance with the structure calculations and Ms. Esther S. H. Lin for her technical assistance with the 2D NMR experiments. This work was supported by a program project grant from Academia Sinica (AS-90-TP-A03) and a grant from the National Science Council of Taiwan (NSC 93-2113-M-001-025). The kinetic experiments carried out in the Larsen group were supported by a grant from the National Science Foundation (NSF MCB0317334).

Supporting Information Available: (Table S1) NMR Assignments of the 19mer. (Figure S1) Reaction scheme for peptide cyclization using the benzoin photolabile-linker strategy. (Figure S2) The PBD signals generated by laser irradiation of the c-19merE11C. This material is available free of charge via the Internet at http://pubs.acs.org.

JA0543191

(36) Dyer, R. B.; Maness, S. J.; Peterson, E. S.; Franzen, S.; Fesinmeyer, R. M.; Andersen, N. H. *Biochemistry* **2004**, *43*, 11560−11566.
(37) Dinner, A. R.; Lazaridis, T.; Karplus, M. *Proc. Natl. Acad. Sci. U.S.A.* **1999**, *96*, 9068−9073.
(38) Du, D.; Zhu, Y.; Huang, C. Y.; Gai, F. *Proc. Natl. Acad. Sci. U.S.A.* **2004**, *101*, 15915−15920.

(39) Abbreviations: 20mer, the Gellman designed peptide with 20 amino acid residues; 20merE12C, the 20mer peptide with E12→C mutation; c-20merE12C, cyclized 20merE12C peptide; 20mer^{D}P6D, the peptide derived from the 20mer and with ^{D}P6→D mutation; 20mer^{D}P6DE12C, the peptide derived from the 20mer^{D}P6D and with E12→C mutation; c-20mer^{D}-P6DE12C, cyclized 20mer^{D}P6DE12C peptide; 19mer, the modified peptide with the VDGO turn sequence instead of the TS^{D}PGK turn sequence in the 20mer peptide; 19merE11C, the peptide derived from the 19mer and with the E11→C mutation; c-19merE11C, cyclized 19merE11C peptide; the letter "O" in the peptide sequence stands for ornithine.